A R C H I V E S O F M E T A L L U R G Y A N D M A T E R I A L S
Volume 59 2014 Issue 4
DOI: 10.2478/amm-2014-0279

D. JANICKI*

DISK LASER WELDING OF ARMOR STEEL

SPAWANIE LASEREM DYSKOWYM STALI PANCERNEJ

The paper describes the application of an Yb:YAG disk laser with a maximum output of 3.3 kW for the butt welding of armor steel plates ARMOX 500T 3.6 mm thick. The influence of laser welding parameters such as laser power beam, welding speed, focal point position on weld quality and mechanical properties of joints was studied. A proper selection of disk laser welding parameters provides non-porous and cracks free fully-penetrated welds with the aspect ratio up to 6.4. There was approx. 40% reduction in the hardness of heat affected zone (HAZ) in comparison to hardness of the base material (BM). The hardness values at the weld metal and the BM were similar. The joints exhibited about 15% lower ultimate tensile strength when compared with that of the BM. Charpy absorbed energy of the joints was approx. 30% lower than that of the BM.

Keywords: laser welding, disk laser, armor steel, Armox 500T, butt joint

Artykuł prezentuje wyniki badań procesu spawania złączy doczołowych blach ze stali pancernej Armox 500T o grubości 3.6 mm, laserem dyskowym Yb:YAG o maksymalnej mocy 3.3 kW. Określono wpływ parametrów spawania tj. mocy wiązki laserowej, prędkości spawania oraz położenia ogniska wiązki laserowej względem spawanej powierzchni na jakość złączy. Wykazano, iż istnieje pole parametrów spawania zapewniające uzyskanie złączy doczołowych wolnych od pęknięć i porowatości oraz współczynniku kształtu spoiny do ok. 6.4. W strefie wpływu ciepła następuje 40% zmniejszenie twardości w stosunku do materiału rodzimego oraz obszary spoiny. Wytrzymałość na rozciąganie złączy jest około 15% niższe od wytrzymałości materiały rodzimego. Udarność złączy jest niższa o 30% od udarności materiału rodzimego.

1. Introduction

High strength quenched and tempered steels (HSQTS) are widely used in military and civil ballistic protection systems. Its applications, ranging from production of armored personnel carriers to building of mobile army installation, e.g. mobile hospitals, result from a beneficial combination of its properties, such as high strength, hardness and ductility and also low price compared to most other armor materials [1-3,10]. Very often above-mentioned applications involve joining by fusion welding methods. However, HSQTS are prone to hydrogen induced cracking and also exhibit heat affected zone (HAZ) softening, what results in poor ballistic performance [1,2, 4-6]. The degree of HAZ softening depends directly on thermal cycle during welding and also chemical and phase compositions of the steel. Therefore, it is desirable to weld HSQTS with low heat input welding processes such as laser beam welding [2,4-6]. The most common welding processes used for production of combat vehicle are shielded metal arc welding (SMAW) and flux cored arc welding (FCAW) [2,4-6].

Currently, laser welding is becoming the leading joining process in various industries, where modern steel grades are used, due to advantages over other welding fusion methods such as high speed, low distortion, low heat input and narrow width of the fusion zone (FZ) and the heat affected zone (HAZ) [7,8,11]. Moreover, the new generation of solid state lasers, namely Yb:YAG disk lasers, provide several benefits for industrial purposes, namely high power with low beam divergence, flexible beam delivery, low maintenance costs, high efficiency and small floor space requirements [9].

The major objective of this study was to investigate the effect of processing parameters on the weld quality in disc laser welding of armor steel ARMOX 500T sheet 3.6 mm thick.

2. Experimental procedure

The base material (BM) was 3.6 mm ARMOX 500T armor steel sheet with the approximate chemical composition shown in Table 1. The BM sheets were laser cut into specimens in dimension of 100×100 mm. Prior to welding the specimens were sandblasted using SiC particles with a diameter of 400-600 μm and washed in acetone.

The experiments of laser butt welding were carried out without filler metal using the Yb:YAG disk laser operating at 1060 nm wavelength in continuous wave mode. The maximum power of laser was 3.3 kW and a beam parameter product (BPP) was 0.8 mm*mrad. The spot diameter of the focused

* SILESIAN UNIVERSITY OF TECHNOLOGY, WELDING DEPARTMENT, 18A KONARSKIEGO STR., 44-100 GLIWICE, POLAND

laser beam was approx. 200 μm. The welding zone was protected by shielding gas – argon at a flow rate of 10 l/min. The cylindrical shielding gas nozzle having a diameter of 10 mm was set at an angle of 45° to the surface of welded specimens and the distance from the welded surface to the nozzle was 10 mm. The specimens were mounted in the stiff clamping device providing backing gas flow (argon) to protect the root side of the weld against atmosphere.

TABLE 1
Chemical composition of steel ARMOX 500T (wt. %)

C	Si	Mn	Cr	Ni	Mo	Fe	P	S	B
0.32	0.40	1.20	1.00	1.80	0.70	bal.	0.015	0.010	0.005

To study the influence of laser welding parameters on the weld bead geometry, microstructure and mechanical properties of the butt joints, the research program was carried out in three stages. First, bead-on-plate welds were prepared at three levels of the laser power, 1500 W, 2000 W and 3300 W, and different welding speeds, ranging from 0.75 m/min to 6.0 m/min. During these welding trials, the laser beam was focused on the top surface of specimens. In the second stage of the experiments, the bead-on-plate welds were made using several negative defocus values (FPP), ranging from 0 mm to -1.5 mm, at constant both laser power of 2000 W and welding speed of 2.0 m/min (Table 2). The third set involved welding of butt joints with optimum parameters (Table 2).

Standard metallographic procedures were used to prepare cross-sections of the bead-on-plate welds and the butt joints for macro and microstructural characterization. Polished sections were etched in Nital at room temperature. Microstructure of weld metal (WM) and heat affected zones (HAZ) were examined using optical microscopy. Geometrical parameters of the welds, such as the weld width and depth, were measured using optical microscope with a Nikon NIS−Elements quantitative image analysis system. The cross-sectional microhardness distribution of the joints was measured by means of Wilson Wolpert 401 MVD Vickers hardness tester at the load of 200 g for a dwell time of 10 s. Microhardness measurements were carried out along the center line at mid-thickness position of the cross-section. Tensile testing was conducted at room temperature and strain rate of 10^{-3} s^{-1} using a Zwick screw-driven universal testing machine. Charpy V-notch impact tests of butt joints and base material (BM) were made at room temperature with under-sized test specimens (3.6 mm thick) using instrumented impact machine AMSLER-RKP 300 with a total capacity of 300 J and a hammer velocity of 5.2 m/s. The V-notch was placed in the center of the weld. Fracture surfaces were examined using scanning electron microscope.

3. Results and discussion

Figure 1 and 2 show the cross-sectional macrographs of bead-on-plate welds produced at the laser power of 2000 and 3300W and welding speeds ranging from 1.0 m/min to 6.0 m/min, while the laser beam was focused on the top surface of specimens. A summary of measurements of bead-on-plate weld geometry is given in Table 2. In all the welding trials, the power density was in the range of 4.8×10^6 to 1.0×10^7W/cm^2, leading to the generation of a keyhole during welding process. As a result, the deep and narrow welds with the high weld aspect ratio (defined as the depth to width ratio) were obtained. The laser power level directly determines the range of welding speed for fully penetrated weld, thus simultaneously determines a minimum heat input level (MHIL) required to achieve a full penetration butt welds. In turn, the welding speed, at given laser power level, has a major effect on the weld aspect ratio (Fig. 3). Generally, with increase of laser power level, both the maximum welding speed (MWS) for fully penetrated weld and the weld aspect ratio increase, whereas the MHIL decreases. The MHIL for fully penetrated bead-on-plate weld was 33 J/mm, at maximum laser power of 3300 W and welding speed of 6.0 m/min. The above-mentioned bead-on-plate weld exhibits also the highest aspect ratio of approx. 6.4. In the range of the investigated welding parameters, the focal point position (FPP) has no significant effect on bead geometry. The minor porosity was observed in the welds produced at the welding speeds lower than 1.0 m/min. These pores are considered to be entrapped shielding gas bubbles, which were formed due to the instability of the keyhole.

The macrographs of the cross section of butt welded joints produced at two levels of heat input, 60 and 120 J/mm, are shown in Fig. 4. The laser butt welding parameters and the measured geometrical parameters of the welds are summarized in Table 2. All the welds are symmetric, fully penetrated and have smooth transition to the base material without undercut or excessive reinforcement. The width of weld face was in the range of 1.1 to 2.6. The weld aspect ratio was found to range from 1.4 to 3.3.

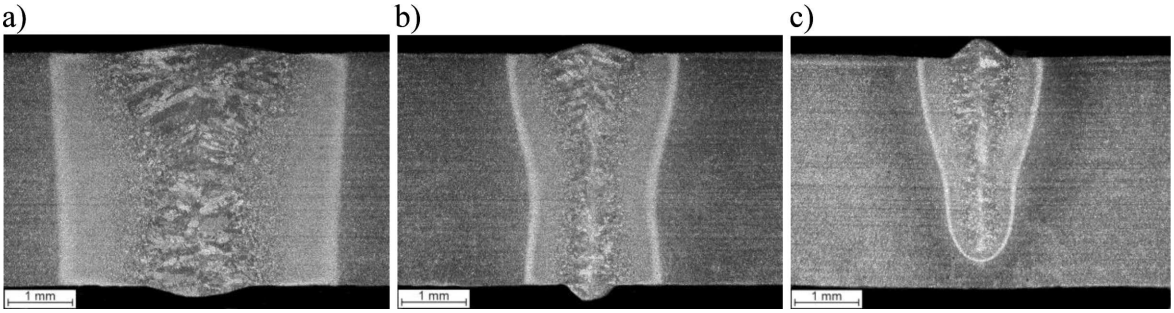

Fig. 1. Macrographs of the cross-section of bead-on-plate welds produced at laser power of 2000 W and different welding speeds: a) 1.0 m/min; b) 2.0 m/min; c) 3.0 m/min (Table 2)

TABLE 2

Parameters of bead-on-plate and butt joints laser welding and measured weld bead dimensions

Bead/joint no.	Laser power W	Welding speed m/min	Heat input* J/mm	FPP** mm	Width of the weld face mm	Width of the weld root mm	Weld depth [mm]	Aspect ratio***
B1	1500	0.75	120	0	2.21	1.23	FP	1.63
B2	1500	1.0	90	0	2.14	0.78	FP	1.68
B3	1500	2.0	45	0	1.35	–	3.09	2.29
B4	2000	1.0	120	0	2.51	1.53	FP	1.43
B5	2000	2.0	60	0	1.35	0.71	FP	2.67
B6	2000	3.0	40	0	0.86	–	3.05	3.55
B7	3300	2.0	99	0	1.38	1.74	FP	2.61
B8	3300	3.0	66	0	1.06	1.14	FP	3.40
B9	3300	4.0	50	0	0.71	1.01	FP	4.80
B10	3300	6.0	33	0	0.56	0.44	FP	6.43
B11	2000	2.0	60	-0.75	1.39	0.72	FP	2.59
B12	2000	2.0	60	-1.50	1.46	0.69	FP	2.47
J1	3000	3.0	60	0	1.11	0.55	FP	3.27
J2	2000	1.0	120	0	2.63	1.66	FP	1.37

Remarks: * defined as the laser power divided by the welding speed, ** – focal point position, *** defined as the depth to width ratio, FP – full penetration weld, B – bead-on-plate weld, J – butt joint

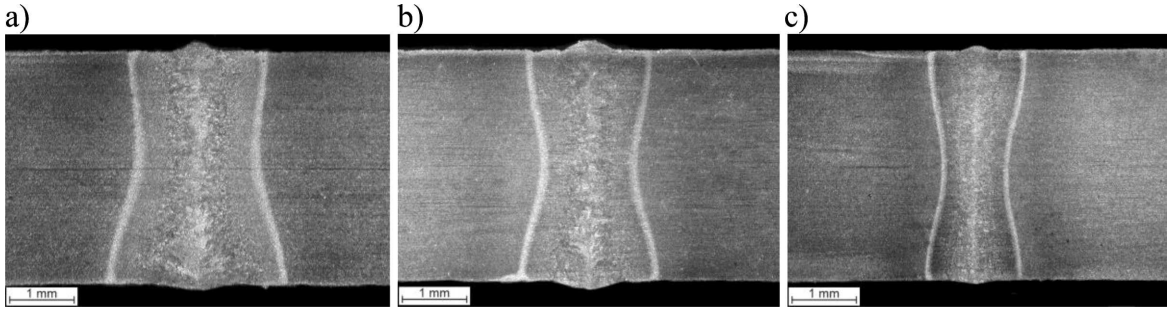

Fig. 2. Macrographs of the cross-section of bead-on-plate welds produced at laser power of 3300 W and different welding speeds: a) 2.0 m/min; b) 4.0 m/min; c) 6.0 m/min (Table 2)

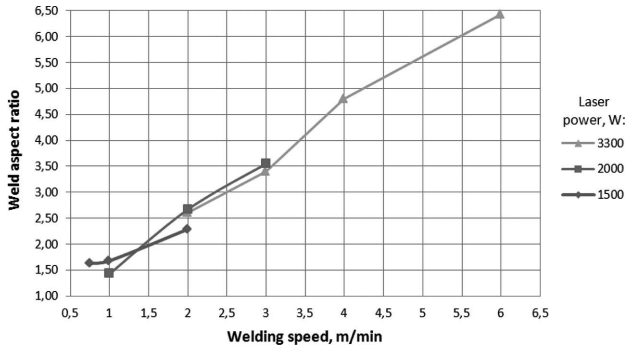

Fig. 3. Plot showing variations in the weld aspect ratio as a function of the laser power and welding speed, while the laser beam was focused on the top surface of specimens (Table 2)

The optical micrographs of base material (BM), heat affected zone (HAZ) and weld metal (WM) of the joints welded at the heat input of 60 and 120 J/mm are presented in Fig. 5 to 8. The corresponding microhardness distribution is shown in Fig. 9. The BM microstructure exhibits tempered martensite with some amount of retained austenite, as shown in Fig. 5. The hardness of the BM was approx. 500 HV. The micrographs taken from the WM of both joints (Fig. 7 and 8) show lath-shaped martensite inside columnar grains, growing along the direction of heat transfer, near the fusion zone boundary (FZB) and inside equiaxed grains in the center of the WM. With decreasing heat input the martensite laths become finer. Additionally, metallographic examination of the joint produced at the lower heat input, Fig. 7, revealed the existence of a relatively planar weld bead centerline grain boundary. The above-mentioned joint exhibits a constant hardness of 530 HV in the WM. Higher heat input leads to lower hardness in the WM, which is attributed to the decrease in both solidification and cooling rates. Moreover, in the case of joints welded at higher heat input, hardness in the WM increases gradually from the weld center and reaches the maximum at the fusion zone boundary (FZB), due to the fact that the temperature gradient is smallest at the weld centerline and greatest at the FZB. Metallographic examination indicates that the HAZ can be roughly divided into three subregions: coarse

grained zone (CGHAZ) adjacent to the FZB, fine grained zone (FGHAZ) and the region close to the BM including subcritical and intercritical zones (SICHAZ), Fig 6. The microstructure within CGHAZ consists of martensite-austenite island in large untempered lath martensite and results from the recrystallization phenomenon occurring in this zone during the welding thermal cycle. The width of this zone was approx. 220 and 480 μm at the heat input of 60 and 120 J/mm, respectively. The hardness of this zone is constant and reaches 550 and 520 HV

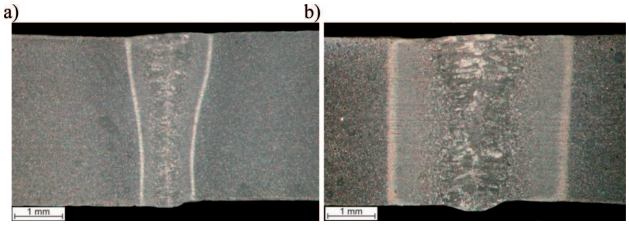

Fig. 4. Macrographs of the cross-section of butt joints produced at the heat input of: a) 60 J/mm; b) 120 J/mm (Table 2)

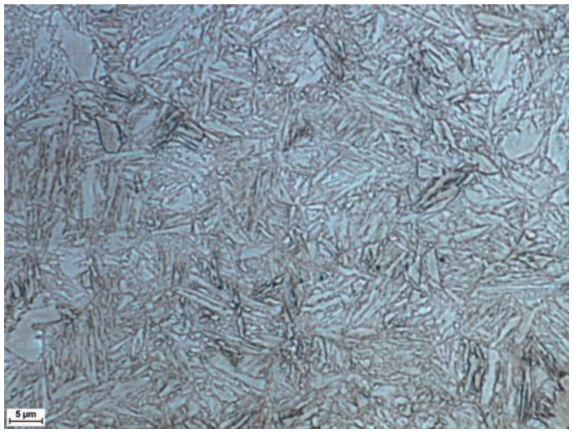

Fig. 5. The microstructure of the base material (ARMOX 500T)

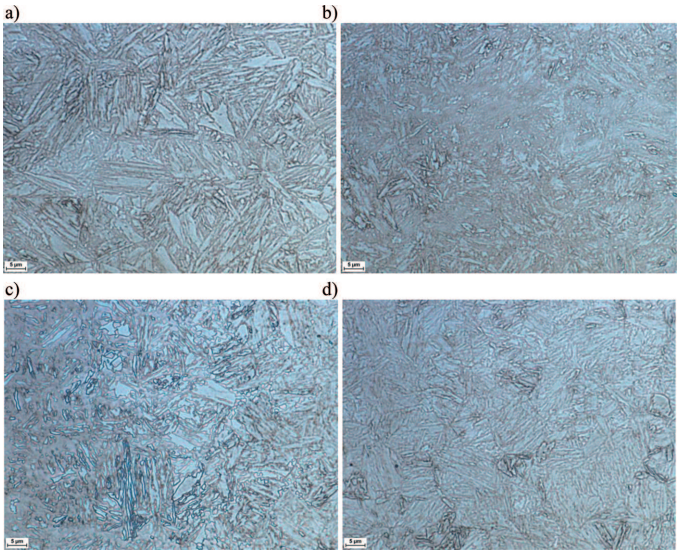

Fig. 6. The HAZ microstructure of the butt joint welded at heat input of 60 J/mm: a) CGHAZ; b) FGHAZ; c) SICHAZ (at the band); d) SICHAZ (next to the band)

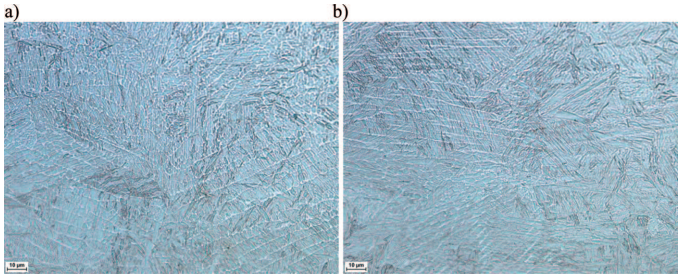

Fig. 7. Microstructure of the butt joint welded at heat input of 60 J/mm: a) the center of the weld metal; b) the weld fusion boundary (from left: weld metal, CGHAZ)

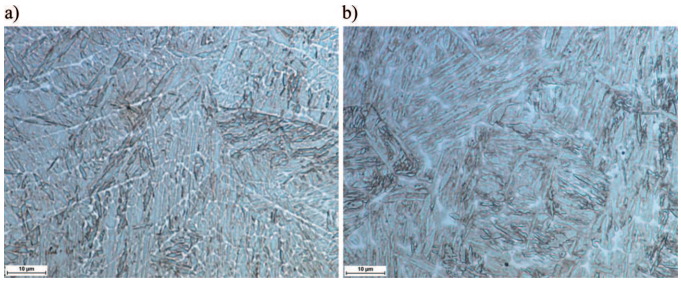

Fig. 8. Microstructure of the center region in the weld metal of butt joints welded at heat input of: a) 60 J/mm; b) 120 J/mm

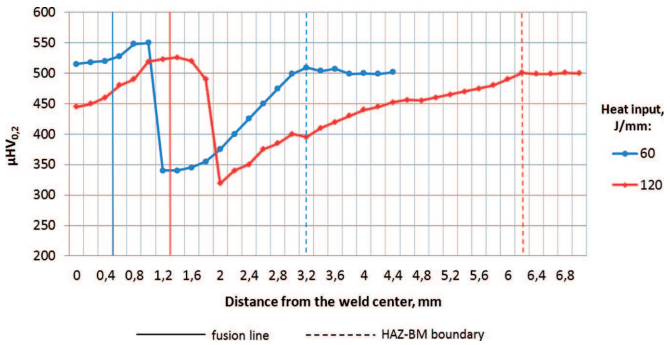

Fig. 9. Microhardness distribution on the cross section of the butt joints

for 60 and 120 J/mm, respectively. Similar values of hardness have been reported in the FGHAZ, which exhibits predominantly very fine untempered martensite. The width of FGHAZ was 150 and 400 μm at 60 and 120 J/mm, respectively. The hardness within SICHAZ decreases sharply to a minimum value of about 320 HV at the white band (Fig. 4 and 6c) and, after passing the white band, the hardness gradually increases up to 500 HV in the BM. Thus, the softest regions of the HAZ was in white bands located in the SICHAZ close to the FGHAZ. The microstructure of these white bands was heavily tempered martensite, possibly with some bainite. The next part of the SICHAZ exhibits tempered martensite. The total width of the SICHAZ was 1.8 and 3.2 mm at the heat input of 60 and 120 J/mm, respectively. No cracks were found in any of the joints and also all of the welds were free of porosity.

Results of mechanical tests of the BM and welded joints are given in Table 3. The mechanical properties of welded joints were examined depending on the heat input level, in the range of 60 and 120 J/mm. All tensile-test weld specimens failed in the HAZ. Nevertheless, it should be noted that the

joints exhibited only about 15% lower ultimate tensile strength when compared with that of the BM. Moreover, it was found that the tensile strength of the joints slightly decreases with increasing the heat input level. The ultimate tensile strength of the joints welded at the heat input of 60 J/mm was about 1500 MPa (only 9% lower than that of the BM), whereas the ultimate tensile strength of the joints welded at 120 J/mm was about 1350 MPa. This indicates 10% reduction in the ultimate tensile strength of the joints. The SEM fractographic investigations of the tensile fracture surface revealed dimple patterns, indicating the ductile fracture mode (Fig. 10). Elongation of all joints was only about 50% of BM elongation. The technological bending test indicated that the joints have poor ductility. The bending angle of all tested joints reached value of 45-50°, both on the weld face and the weld root, whereas the BM achieved 180° deflection without cracks. All joints during bending test were broken in the HAZ. The fracture surface of the joints welded at 120 J/mm shown the ductile fracture mode, however, in the case of joints welded at 60 J/mm the mixed ductile/brittle fracture mode was observed, Fig. 11.

The mean Charpy absorbed energy values of the BM and joints welded at two levels of the heat input are given in Table 3. The results of Charpy impact test indicate that the impact properties of the joints are significantly lower than that of BM and directly depend on the heat input level. The Charpy absorbed energy of the joints welded at the higher heat input (120 J/mm) is approx. 30% lower than that of BM. The reduction of heat input leads to further decrease of Charpy absorbed energy of the joints. In the case of joints welded at the lower heat input (60 J/mm) the Charpy absorbed energy was only about 50% of the BM absorbed energy. The higher impact properties of the joints welded at the heat input of 120 J/mm were associated with failure by microvoid coalescence, whereas the joints welded at lower heat input exhibited a mixed mode of fracture of microvoid coalescence and cleavage, Fig. 12.

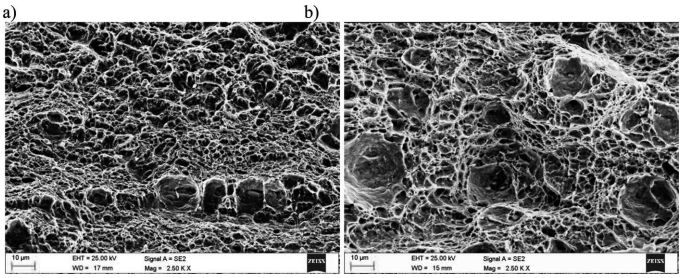

Fig. 10. SEM micrographs of fracture surface after tensile tests of the joints welded at the heat input of: a) 60 J/mm; b) 120 J/mm

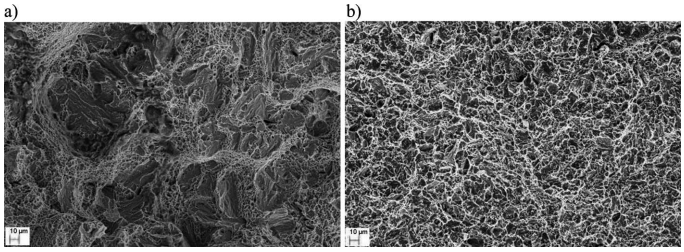

Fig. 11. SEM micrographs of fracture surface after bending tests of the joints welded at the heat input of: a) 60 J/mm; b) 120 J/mm (magnification 2500x)

TABLE 3

Results of mechanical tests of the BM and the welded joints

Material/ joint no. (Table 2)	**Tensile test**			**Bending test**			**Charpy impact test**
	Ultimate tensile strength MPa	Elongation %	Location of failure*	Test type	Bending angle	Remarks/ location of failure*	Absorbed energy J
J1	1499	3.8	HAZ	face bend	46°	HAZ	12
				root bend	55°	HAZ	
J2	1348	4.0	HAZ	face bend	45°	HAZ	18
				root bend	47°	HAZ	
Base material	1645	8.1	–	–	180°	no crack	26

Remarks: J1 – 60 J/mm, J2 – 120 J/mm, * HAZ – heat affected zone

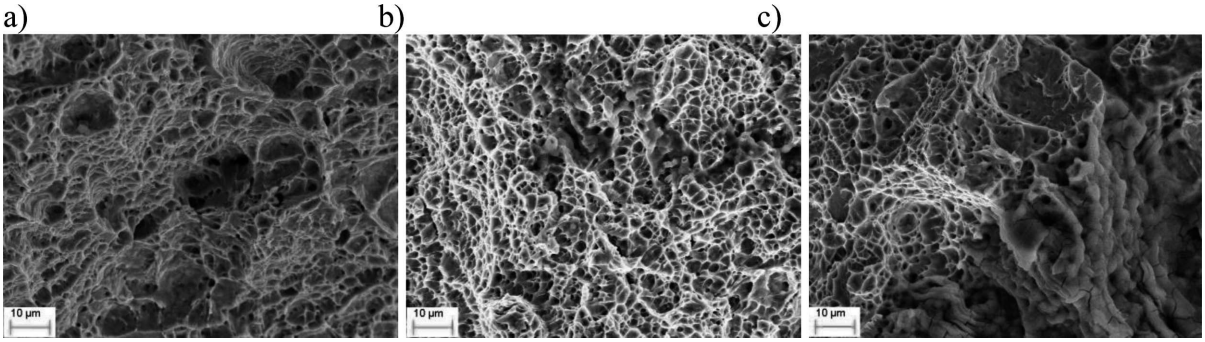

Fig. 12. Appearance of the fracture of Charpy specimens: a) BM; b) joint welded at the heat input of 120 J/mm; c) joint welded at 60 J/mm. SEM (magnification 2500x)

4. Conclusions

The keyhole laser welding without filler metal using the Yb:YAG disk laser allows to produce high quality butt joints of 3.6 mm ARMOX 500T armor steel sheets. The laser power level directly determines the range of welding speed for fully penetrated weld, thus simultaneously determines a minimum heat input level required to achieve a full penetration butt welds. In turn, the welding speed has a major effect on the weld aspect ratio. A proper selection of laser welding parameters provides non-porous and crack-free welds with the aspect ratio up to 6.4. The minimum heat input required to achieve full penetration butt welded joints with no defects was found to be 60 J/mm.

The hardness values at the weld metal and the BM were similar. By contrast, the HAZ can be roughly divided into two regions: zone adjacent to the fusion line exhibited slightly higher hardness when compared with that of the BM and softened zone close to the BM. The hardness of the softened zone was approx. 40% lower in comparison to hardness of the BM, independently of the heat input. In turn, the width of the softened zone depends on the heat input level, and was approx. 1.8 mm and 3.2 mm at the heat input of 60 and 120 J/mm, respectively.

The joints exhibited only about 15% lower ultimate tensile strength when compared with that of the BM. The tensile strength of the joints slightly decreases with increasing the heat input level. Moreover, it was found that the effect of the heat input on the impact properties of the joints is significant. The reduction of heat input leads to decrease of Charpy absorbed energy of the joints. The Charpy absorbed energy values of the joints welded at the heat input of 120 and 60 J/mm were approx. 30% and 50% lower than that of BM, respectively.

REFERENCES

[1] I. Barényi, O. Híreš, P. Lip, Changes in Mechanical Properties of Armoured UHSLA Steel ARMOX 500 After Over Tempering. PROBLEMS OF MECHATRONICS ARMAMENT, AVIATION, SAFETY ENGINEERING. (14), 7-14 (2013).

[2] G. Magudeeswaran, et al., Effect of welding consumables on tensile and impact properties of shielded metal arc welded high strength, quenched and tempered steel joints. Journal of iron and steel research, international **15**, 87-94 (2008).

[3] T. Borvik, S. Dey, A.H. Clausen, Perforation resistance of five different high strength steel plates subjected to small arm projectiles. Int J of Impact Eng **36**, 948-964 (2009).

[4] S.J. Alkemade, The Weld Cracking Susceptibility of High Hardness Armour Steel. Australia: Defence Science and Technology Organization, 1996.

[5] D. Wojnowski, Y.K. Oh, J.E. Indacochea, Metallurgical Assessment of the Softened HAZ Region During Multipass Welding Journal of Manufacturing Science and Engineering **122**(2), 310 (2000).

[6] G. Madhusudhan, et al., Effect of Welding Process on the Ballistic Performance of HighStrength Low-Alloy Steel Weldments. Journal of Materials Processing Technology **74**(1-3), 27 (1998).

[7] A. Lisiecki, Diode laser welding of high yield steel', Proc. of SPIE, Vol. 8703, Laser Technology 2012: Applications of Lasers, 22 January 2013, 223-234.

[8] D. Janicki, Fiber laser welding of nickel based superalloy Inconel 625', Proc. SPIE, Laser Technology 2012: Applications of Lasers, 2013, 8703, 87030R, doi: 10.1117/12.2013430.

[9] A. Lisiecki, Welding of titanium alloy by Disk laser. Proc. of SPIE Vol. 8703, Laser Technology 2012: Applications of Lasers, 87030T (January 22, 2013).

[10] W. Burian, J. Marcisz, B. Garbarz, L. Starczewski, Nanostructured Bainite-Austenite Steel for Armours Construction, Archh. Metall. Mater. **59**(3), 1211-1216 (2014).

[11] A. Grajcar, M. Różański, M. Kaminska, B. Grzegorczyk, Study on Non-Metallic Inclusions in Laser-Weided TRIP-Aided Nb-Microalloyed Steel, Arch. Metall. Mater. **59**(3), 1163-1169 (2014).

Received: 10 October 2013.